Proceedings of ASME Turbo Expo 2011
GT2011
June 6-10, 2011, Vancouver, British Columbia, Canada

GT2011-45647

# IMPACT OF SEVERE TEMPERATURE DISTORTION ON TURBINE EFFICIENCY

**Paul F. Beard†, Andy Smith*, Thomas Povey†**

†Dept. Eng. Science, University of Oxford , Parks Road , Oxford, OX1 3PJ, UK
*Rolls-Royce PLC, Turbine Systems, PCF-1, PO Box 31, Moor Lane, Derby, DE24 8BJ, UK

## ABSTRACT

This paper presents an experimental and computational study of the effect of severe inlet temperature distortion (hot streaks) on the efficiency of the MT1 HP turbine, which is a highly-loaded unshrouded transonic design.

The experiments were performed in the Oxford Turbine Research Facility (OTRF) (formerly the TTF at QinetiQ Farnborough): an engine scale, short duration, rotating transonic facility, in which $M$, Re, $T_{gas}/T_{wall}$ and $N/\sqrt{T_{01}}$ are matched to engine conditions. The research formed part of the EU Turbine Aero-Thermal External Flows (TATEF II) programme.

An advanced second generation temperature distortion simulator was developed for this investigation, which allows both radial and circumferential temperature profiles to be simulated. A pronounced profile was used for this study. The system was novel in that it was designed to be compatible with an efficiency measurement system which was also developed for this study. To achieve low uncertainty (bias and precision errors of approximately 1.5 per cent and 0.2 per cent respectively, to 95 per cent confidence), the mass flow rate of the hot and cold streams used to simulate temperature distortion were independently metered upstream of the turbine nozzle using traceable measurement techniques. Turbine power was measured directly with an accurate torque transducer.

The efficiency of the test turbine was evaluated experimentally for a uniform inlet temperature condition, and with pronounced temperature distortion. Mechanisms for observed changes in the turbine exit flow field and efficiency are discussed. The data are compared in terms of flow structure to full stage CFD performed using the Rolls Royce Hydra code.

## INTRODUCTION

For a gas turbine engine, it is thermodynamically beneficial to raise the turbine inlet temperature. By doing so, the cycle efficiency and specific work output increase resulting in improved specific fuel consumption.

Non-uniform temperature patterns (or so-called distortion) at the inlet to the high-pressure turbine arises from discrete burners and dilution air jets and endwall cooling flows.

Many experimental studies have been conducted on the effect of inlet temperature distortion on turbine aerodynamics and heat transfer. There exist a number of articles reviewing these investigations and the experimental generation of inlet temperature distortion: [1], [2], [3].

One of the first experiments performed to study the impact of inlet temperature distortion was conducted by Butler *et al*. [4]. The vane flow-field was found to be unaffected by the hot-streak, a result that confirmed the theoretical analysis of Munk and Prim [5], who noted that the inviscid streamline pattern in a stationary blade is only influenced by non-uniformities of inlet total pressure. The flow-field in the rotor passage, however, was significantly affected by the hot-streak. Results indicated the hot and cold regions of gas were segregated in the rotor passage, with hot gas collecting on the pressure surface and cold gas collecting on the suction surface, an effect first observed in compressors by Kerrebrock and Mikolajczak [6]. Strengthened rotor secondary flows also resulted in stronger radial transport in the rotor passage. Unlike in the stationary vane passage, Hawthorne [7] showed that the production of secondary vorticity is dependent on the presence of temperature gradients.

The first measurements of the effect of inlet hot-streaks on rotor heat transfer in a transonic turbine were conducted by Shang *et al*. [8]. A strong migration of hot gas towards the hub endwall in the rotor passage was observed. Shang and Epstein [9] performed complementary CFD simulations, concluding that the migration of hot gas towards the hub was caused by a buoyancy effect. The computation also showed that the introduction of hot-streaks caused a pitchwise variation in the time-average of total temperature at the rotor inlet, which resulted from the unsteady fluctuations of the NGV exit flow angle as the rotor passes.

 

To date, perhaps the most comprehensive turbine stage heat transfer measurements with inlet temperature distortion were conducted in the Oxford Turbine Research Facility (OTRF). These experiments included investigations into the effect of clocking – measurements were performed with the hot-streaks aligned with the leading edge and mid-passage of the HP vane. Povey *et al*. [2] compared heat transfer results on the NGV surfaces and endwalls with inlet hot-streaks (including clocking) against those with a uniform inlet temperature profile. These results showed an increase in heat transfer on the NGV suction surface with the hot-streak aligned with its leading edge and a significant reduction in heat transfer on the endwalls in both clocking positions. Chana and Jones [10] showed a decrease in the heat transfer on the rotor tip and casing in both clocking positions. Povey *et al*. [11] reported heat transfer measurements on the surfaces of a downstream IP vane. An approximate 20% rise in heat transfer was observed. Most recently, Qureshi *et al*. [12] have presented heat transfer measurements and computations on the rotor surfaces with a pronounced heat-streak profile. Significant changes in heat flux were observed and primarily attributed to changes in local adiabatic wall temperature rather than heat transfer coefficient.

This paper presents the first detailed experimental and computational study of the impact of engine-representative combustor hot-streaks on the efficiency of a high-pressure transonic turbine. It is hoped that the results will enable better understanding of turbine behaviour with inlet distortions and allow for improvements in turbine efficiency and durability.

## THE OXFORD TURBINE RESEARCH FACILITY

A schematic of the Oxford Turbine Research Facility (OTRF) is shown in Figure 1 below. The OTRF is a short-duration, rotating, isentropic light piston turbine facility used for engine representative aerodynamic and heat transfer investigations of single-stage (HP vane and rotor) or 1½ stage (HP stage and IP/LP vane) turbines. For this study, the OTRF was configured as a single stage turbine. The turbine was the full-scale highly-loaded unshrouded transonic MT1 stage. The matched operating conditions are summarised in Table 1.

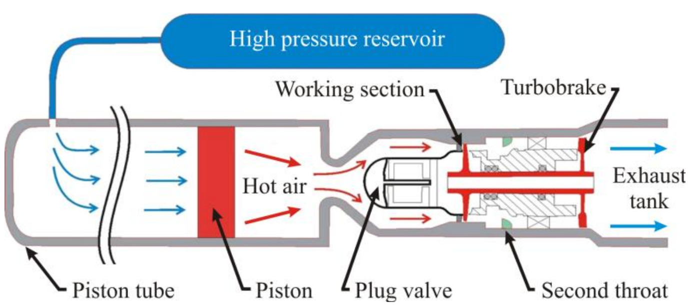


**FIGURE 1: The Oxford Turbine Research Facility (OTRF)**

The fundamental operation of this type of facility was first described by Jones *et al*. [13]. The test gas (air) in the OTRF is contained in the large piston tube (volume ~10 m$^3$) in front of a light-free piston. This air is compressed, and hence heated, by the action of high-pressure air injected into the pump tube behind the piston.

The total pressure and total temperature at inlet to the turbine are approximately constant during a run. A unique feature of the OTRF is the aerodynamic braking system [14], or turbobrake, which maintains turbine speed during a test run. The turbine pressure ratio is set by an adjustable choked throat downstream of the stage. A steady run time of approximately 400 ms can be achieved at the conditions relevant to the reported tests.

| PARAMETER | VALUE |
|---|---|
| Re based on NGV axial chord | 1.61 x 10$^6$ |
| Mach number at NGV exit | 0.879 |
| Capacity, $\dot{m}\sqrt{T_{01}}/p_{01}$ | 7.97x10$^{-4}$ kg s$^{-1}$ K$^{½}$ Pa$^{-1}$ |
| Corrected speed, $N/\sqrt{T_{01}}$ | 451.3 rpm K$^{-½}$ |
| Inlet total temperature | 444 K |
| Inlet total pressure | 4.6 x 10$^5$ Pa |
| Pressure ratio, $p_{01}/p_{3,hub}$ | 3.219 |
| Gas-to-wall temperature ratio | 1.52 |

**TABLE 1: MT1 operating point in the OTRF**

## INLET HOT-STREAK GENERATION

The development and implementation of an enhanced (second generation) inlet temperature distortion, or EOTDF, generator was described by Povey and Qureshi [15]. The generator was designed to produce a pronounced temperature profile, representative of an extreme operating point in a modern engine cycle.

The temperature profile is generated by the controlled introduction of hot and cold gas upstream of the turbine stage. The facility is operated to achieve the same mass-averaged values of inlet total temperature (444 K) and pressure (4.6 bar) with and without EOTDF. The hot-streak to vane count ratio is 1:1. The temperature profiles measured across 2 NGV pitches at the turbine inlet with and without EOTDF are compared in Figure 2 below. These measurements were conducted by traversing fixed radial rakes of 25.4 μm diameter bare-bead k-type thermocouples across the survey area over a number of test runs (circles indicate measurement locations). A standard deviation of ±0.46% in the data without hot-streaks generation demonstrated a particularly uniform profile. With hot-streak generation, the maximum-to-mean and maximum-to-minimum temperature ratios were 1.18 and 1.81 respectively. The design circumferential variation ($T_{max}/T_{min}$ = 1.08, $T_{max}/T_{mean}$ = 1.06) was weak in comparison to radial variation.

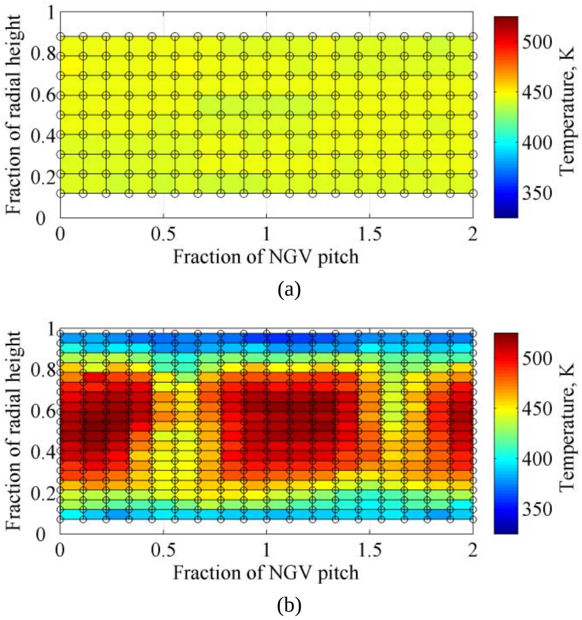


**FIGURE 2: Measured stage inlet temperature profile with: (a) uniform inlet conditions, (b) inlet hot-streak generation**

The total pressure profiles measured at the stage inlet with and without inlet hot-streaks were presented by Povey and Qureshi [15]. The mass-averaged values for these profiles were 4.593 bar and 4.598 bar respectively, with standard deviations in the data of ±0.15% and ±0.13% respectively. The excellent similarity between these profiles was important, as resulting changes in turbine heat transfer and aerodynamics could be solely attributed to the introduction of the hot-streak profile.

## TURBINE EFFICIENCY MEASUREMENT SYSTEM

The development of a turbine efficiency measurement system for the OTRF was described by Beard *et al.* [16]. Turbine efficiency measurements performed with the MT1 turbine with uniform inlet conditions of $p_{01}$ and $T_{01}$ were presented by Beard *et al.* [17]. The measurements with inlet temperature distortion followed the same method.

To determine turbine efficiency in a transient facility, the heat transferred from the working fluid must be accounted for (usually $T_{gas} > T_{wall}$). In a non-adiabatic situation, the rational definition of turbine efficiency is with reference to a process with the same heat transfer as the real process, but with no irreversibilities that would give rise to additional entropy. That is, the reference process is non-isentropic but nonetheless reversible. The ideal non-adiabatic reference process and actual non-adiabatic expansion process are shown on the *h*-*s* in Figure 3 below. The isentropic process is also plotted. Throughout this paper subscripts 1 to 4 are used to identify the four main measurement planes: NGV inlet plane (subscript 1); NGV exit/HP rotor inlet plane (subscript 2); the HP rotor exit near and far planes (subscripts 3 and 4 respectively).

By considering the *h*-*s* chart in Figure 3, it can be shown that the efficiency of a turbine tested in a non-adiabatic situation, such as in the OTRF, can be expressed as:

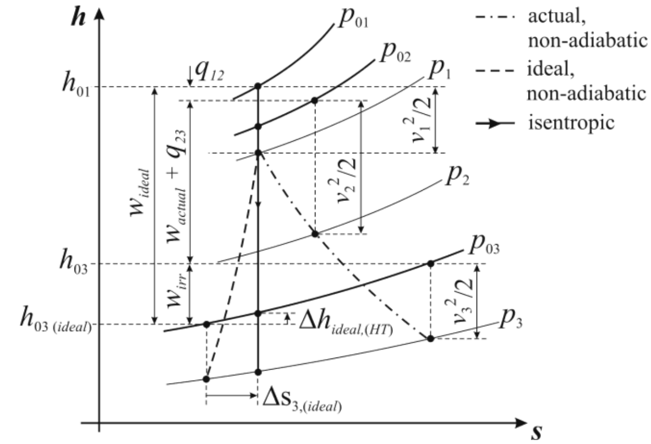


**FIGURE 3: Enthalpy-entropy chart showing isentropic and non-adiabatic turbine expansions**

$$\eta = \frac{\dot{W}_{ideal} - \dot{W}_{irr}}{\dot{W}_{ideal}} = \frac{\dot{H}_{01} - \dot{H}_{03}}{\dot{H}_{01} - \dot{H}_{03,ideal}} = \frac{\dot{W}_{actual} + \dot{Q}_{13}}{\dot{W}_{is} + \Delta\dot{H}_{ideal,(HT)}} \qquad (1)$$

where $\dot{Q}_{13}$, is the stage heat transfer between planes 1 and 3, and $\Delta\dot{H}_{ideal,(HT)}$ is the change in the exit total enthalpy flux – from isentropic – as a result of this heat transfer.

The OTRF efficiency measurement system uses a direct measurement of shaft torque, $T_{gauge}$, using strain gauges and rotational speed to determine the actual power extracted by the turbine. Small corrections were applied for disc windage (~1.7% of $T_{gauge}$) and the inertial torque (~0.4% of $T_{gauge}$) due to small changes in the rotational speed during the test run. The isentropic turbine power was determined from the measurement of stage mass flow rate and by considering such an expansion from the stage inlet conditions of $p_{01}$ and $T_{01}$ across the stage total-to-total pressure ratio. The system allows efficiency measurements to be determined based on area-traverse measurements at two rotor exit planes. The *near* and *far* planes were 0.5 and 4.5 mid height axial chords from the rotor trailing edge. The turbine efficiencies evaluated using the traverse data acquired at these two rotor planes are given by:

$$\eta_{near} = \frac{\left(T_{gauge} + T_{wind} + I_{rotor}\dot{\omega}\right)\omega + \dot{Q}_{13}}{\dot{m}c_p\bar{T}_{01}\left\{1 - \left(\frac{\bar{p}_{03}}{\bar{p}_{01}}\right)^{(\gamma-1)/\gamma}\right\} + \Delta\dot{H}_{ideal,(HT)}} \qquad (2)$$

$$\eta_{far} = \frac{\left(T_{gauge} + T_{wind} + I_{rotor}\dot{\omega}\right)\omega + \dot{Q}_{13}}{\dot{m}c_p\bar{T}_{01}\left\{1 - \left(\frac{\bar{p}_{04}}{\bar{p}_{01}}\right)^{(\gamma-1)/\gamma}\right\} + \Delta\dot{H}_{ideal,(HT)} - \dot{Q}_{34} - \Delta\dot{H}_{BL}} \qquad (3)$$

where $\dot{Q}_{34}$ is the heat transferred to the exit duct surfaces and $\Delta\dot{H}_{BL}$ is the drop in total enthalpy flux resulting from boundary layer growth down the exit duct ($\Delta\dot{H}_{34} = \dot{Q}_{34} + \Delta\dot{H}_{BL}$). The growth of the exit duct boundary layer causes a reduction in total pressure, which respectively increases and decreases the determined values of isentropic turbine power and turbine efficiency. The difference in the turbine efficiency values measured between the rotor exit traverse planes due to the boundary layer growth down the exit duct was estimated at -0.15% by Beard *et al*. [17].

SHAFT TORQUE MEASUREMENT

The shaft torque measurement system developed for the OTRF is detailed by Beard and Povey [18]. This system uses 16 strain gauges mounted on the hub of the turbine disc to provide a direct measurement of the extracted torque. The strain gauge system was calibrated against a traceable reference transducer with a nominal accuracy of ±0.03%. Thermal calibrations were also conducted. A windage correlation for the MT1 rotor disc was determined from a series of spin-down experiments (without the rotor blades and turbobrake) conducted over a range of rotor cavity pressures. Typically, disc windage caused a maximum reduction in shaft torque of approximately 1.7% during a test run. Small changes in rotational speed during the test run caused a small inertial torque of approximately 0.4% of $T_{shaft}$. The angular acceleration of the rotor, $\dot{\omega}$, was determined from the numerical differentiation of the angular velocity measurement. The bias and precision uncertainties associated with the torque measurement system were ±0.117% and ±0.198% respectively.

STAGE MASS FLOW RATE MEASUREMENT

The turbine stage mass flow rate was measured using the piston tube exit contraction as a subsonic venturi upstream of the turbine. This measurement system is fully detailed by Beard *et al*. [19]. A small correction (∼±0.4% of $\dot{m}$) for the change in stored mass between the piston tube exit contraction and the turbine stage was performed. The leakage through the rotor seals was approximately ±0.01% of $\dot{m}$. The single test precision and bias uncertainties associated with the measurement of the stage mass flow rate were ±0.47% and ±1.29% respectively.

With the generation of inlet hot-streaks, the cold stream mass flow rate was independently metered by a calibrated (traceable) sonic venturi before entering the rig module [19]. The bias uncertainty associated with the measurement of the cold stream mass flow rate was ±0.61%. The target cold and hot stream mass flow rates were 6.26 kg s$^{-1}$ and 11.14 kg s$^{-1}$. Therefore with inlet hot-streaks, the bias uncertainty in the measurement of stage mass flow rate was estimated at ±0.85%. Treating air as a fluid, the variation in $c_p$ varied by approximately 2.8% across the inlet plane. Consequently with EOTDF, $T_{01}$ was averaged by conserving inlet total enthalpy:

$$\bar{T}_{01,EOTDF} = \frac{\left(\dot{m}c_pT_0\right)_{cold} + \left(\dot{m}c_pT_0\right)_{hot}}{\left(\dot{m}_{cold} + \dot{m}_{hot}\right)\bar{c}_p} \tag{4}$$

where $\bar{c}_p$ is the mass-averaged value at the inlet plane.

INLET AREA-SURVEYS

Inlet area-surveys of $p_{01}$ and $T_{01}$ were conducted by incrementally traversing radial rakes across two vane passages. Total pressure measurements were conducted using rakes of nine Kiel head pitot tubes with diaphragm-based transducers connected to pneumatic lines. Total temperature measurements were performed using 25.4 μm diameter bare-bead k-type thermocouples mounted in ceramic inserts. The frequency response requirements for these measurements were discussed by Beard *et al*. [16]. The bias and precision measurement uncertainties associated with $\bar{p}_{01}$ and $\bar{T}_{01}$ were less than ±0.1%.

EXIT AREA-SURVEYS

Area-surveys of $p_0$, $M$, yaw angle and $T_0$ were conducted at rotor exit near and far planes at 17 radial heights. A three-hole probe with two nose-mounted 12.7 μm diameter aspirated thermocouples was used. Compressible calibrations for these probes were determined using a transonic wind tunnel over a Mach number range of $0.2 < M < 1.2$. With a traverse time of 200 ms, the near and far probe response errors were estimated at ±0.84% and ±0.56% respectively. The errors in the mass-weighted values of $p_0$ at the near and far planes were estimated at ±0.042% and ±0.037% respectively.

The area-survey of $p_{03}$ with inlet hot-streaks is shown in Figure 4. Measurements between 12.5% and 93% span were possible. The impact of the vane secondary flows, which were transported through the rotor, was observed as regions of low $p_0$ (and Mach number). A strip of relatively high $p_0$ across the full vane spacing above 90% span can be attributed to the influence of tip leakage.

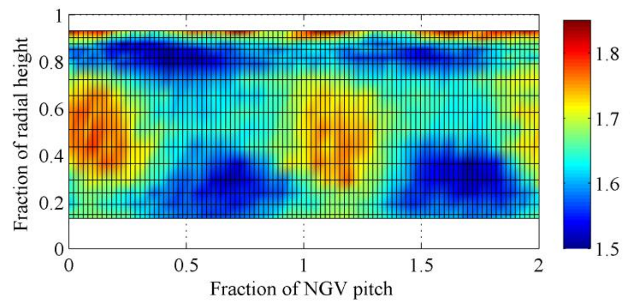


**FIGURE 4: Rotor exit near plane area-survey results of total pressure, $p_{03}$, with inlet hot-streaks.**

The area-survey of $p_{04}$ with inlet hot-streaks is shown in Figure 5 (with the same scale as Figure 4). Measurements between 4% and 96% span were possible. Mixing has reduced variations in $p_0$, but the influence of the vane wakes is still clear. Area-survey results of $p_{03}$ and $p_{04}$ with uniform inlet conditions were presented by Beard *et al*. [17].

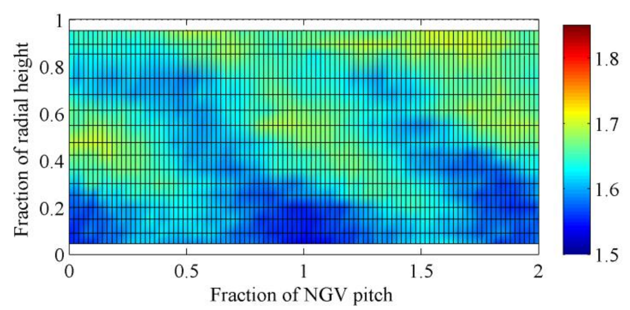


**FIGURE 5: Rotor exit far plane area-survey results of total pressure, $p_{04}$, with inlet hot-streaks**

NON-ADIABATIC TERMS

The stage heat transfer, $\dot{Q}_{13}$, was estimated from extensive thin-film gauge measurements. With uniform inlet conditions, $\dot{Q}_{13}$ was estimated at 100.7 kW from the measurements by Chana and Hilditch [20] and Chana and Jones [10]. With inlet hot-streaks, $\dot{Q}_{13}$ was estimated at 81.4 kW from the measurements by Qureshi *et al*. [12], [21].

On an *h-s* chart, the gradient of an isobar is equal to the gas temperature. Therefore, $\Delta\dot{H}_{ideal,(HT)}$ can be determined by considering the change in the fluid entropy resulting from the heat transferred to the turbine surfaces:

$$\Delta\dot{H}_{ideal,(HT)} = \dot{H}_{is} - \dot{H}_{03,ideal} \sim T_{03,is}\int_{3,ideal}^{3,is} ds \qquad (5)$$

The integration in equation (5) was approximated using a simple method presented by Atkins and Ainsworth [22], in which the heat transfer is assumed to occur at the inlet temperature in the NGV passage, and at the mean temperature between the inlet and exit of the stage in the rotor passage:

$$\Delta\dot{H}_{ideal,(HT)} \sim T_{03,is}\left\{\frac{\dot{Q}_{12}}{\bar{T}_{01}} + \frac{\dot{Q}_{23}}{\frac{1}{2}(\bar{T}_{01}+\bar{T}_{03})}\right\} \qquad (6)$$

The uncertainty in the correction for non-adiabatic test conditions is dominated by the error in the measurements of heat transfer rate, which was estimated at approximately ±10%. The correction corresponded to approximately 1.6% in turbine efficiency. Therefore, the uncertainty in the application of the correction was small at ±0.16%.

## COMPUTATIONAL SCHEME

A computational study of the impact of engine-representative hot-streaks on the performance of the MT1 HP turbine was conducted using the Rolls-Royce HYDRA solver [23] with the Spallart-Allmaras turbulence model. The solver used an edge-based difference method with a second order discretisation scheme. An implicit dual-time stepping scheme was adopted for the unsteady computations. Steady flow solutions were obtained using the mixing-plane technique with a non-reflective vane/rotor interface. Unsteady solutions were computed using a sliding plane interface with a single cell overlap to improve the flux conservation between the vane and rotor domains.

The MT1 turbine stage with 32 vanes and 60 blades (32:60) was modelled as 32:64. This provided a sizeable reduction in the computational time as a computational domain of 1:2 could be modelled rather than 8:15. Compensation for the effect of changing the vane-to-blade count ratio on the stage work function and capacity was performed by skewing open the rotor geometry by 0.82°. The computational domain extended from the stage inlet plane to the rotor exit far plane.

The computational grid was generated by the Rolls-Royce PADRAM (Parametric Design RApid Meshing) software. This is a structured multi-block mesh generator which produces an ‘O’ mesh around the aero-foil and an ‘H’ mesh elsewhere. A mesh density of 0.75 million cells per vane passage and 0.97 million cells per rotor passage was used. Wall functions were imposed on the solid boundaries, and the mean $y^+$ value was approximately 20. The vane and rotor surface meshes are shown in Figure 6 below.

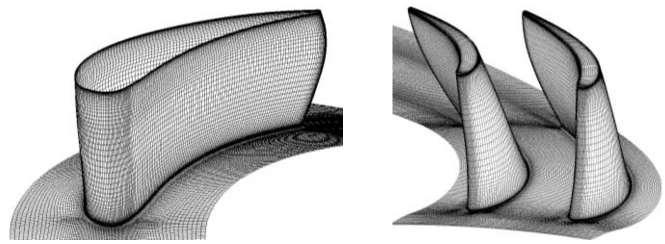

**FIGURE 6: Vane and rotor computational meshes**

The computational boundary conditions were matched to the experimental conditions: $p_{01}$ = 4.6 bar; $T_w$ = 288 K; $N$ = 9500 rpm. The results from the Rolls-Royce through-flow code, Q263, were used to define the radial static pressure distribution at the rotor exit. With the case with uniform inlet conditions, $T_{01}$ was set to 444 K. With inlet hot-streaks, the inlet boundary condition of $T_{01}$ was set to the match the generated profile shown in Figure 2(b).

## EXPERIMENTAL TURBINE EFFICIENCY RESULTS

The impact of EOTDF is summarised in Table 2, and compared to the uniform inlet condition. Turbine efficiency was evaluated based on near and far plane measurements, for mass-averaged and mixed-out conditions. The mixing model of Dzung (see [24]) was used. The measurement bias, $B_x^{95\%}$, and precision uncertainties, $S_x^{95\%}$, are also listed in Table 2. Superscript 1 indicates conditions with EOTDF. Superscript 2 indicates the uncertainty in the mean value from 15 tests runs.

| Parameter | Uniform | EOTDF | $S_x^{95\%}$ | $B_x^{95\%}$ |
|---|---|---|---|---|
| Shaft torque, $T_{rotor}$ | 1692.1 Nm | +0.47% | ±0.20% | ±1.02% |
| Mass flow rate, $\dot{m}$ | 17.04 kg s$^{-1}$ | +0.94% | ±0.47% | ±1.29%<br>±0.85% [1] |
| $\bar{T}_{01}$ | 444 K | 0% | ±0.13% | ±0.32% |
| $\bar{p}_{03}/\bar{p}_{01}$ | 0.3550 | +0.51% | ±0.10% | ±0.84% |
| $\bar{p}_{04}/\bar{p}_{01}$ | 0.3513 | +0.65% | ±0.10% | ±0.58% |
| Shaft power, $\dot{W}_{actual}$ | 1.683 MW | +0.47% | ±0.20% | ±0.12% |
| Isentropic power, $\dot{W}_{is}$ | 1.959 MW | +0.81% | ±0.50% | ±1.45%<br>±1.08% [1] |
| $\dot{Q}$ correction | +2.06% | -0.34% | ±0.02% | ±0.24% |
| $\eta_{mass,near}$ | 88.63% | -0.51% | ±0.64%<br>±0.16% [2] | ±1.49%<br>±1.08% [1] |
| $\eta_{Dzung,near}$ | 88.11% | -0.88% | | |
| $\eta_{mass,far}$ | 88.21% | -0.41% | ±0.64%<br>±0.16% [2] | ±1.45%<br>±1.08% [1] |
| $\eta_{Dzung,far}$ | 87.98% | -0.68% | | |

**TABLE 2: Impact of introducing EOTDF profile at inlet to MT1 turbine: experimental results**

The near-wall flow-fields absent in the measured area-survey data, including the influence of low momentum regions in the boundary layer and the high-momentum tip leakage region, were accounted for using a patching method, relying on trends (but not absolute values) predicted using CFD [17]. This allowed the gross effects to be accounted for. The mass flux in the patched near wall regions is relatively small, reducing the inherent uncertainty introduced by this method. At the rotor exit far plane, the difference in the mass-averaged turbine efficiency determined using the 'patched' traverse data and the measured data between 4% and 96% span was +0.16%. At the near plane the corresponding difference was -0.45%. It can reasonably be assumed that the error introduced by using this method of accounting for the near wall flow is significantly smaller than the difference introduced by correcting.

With the introduction of inlet hot-streaks and a mass-averaged pressure ratio, changes in turbine efficiency (from the test case with uniform inlet conditions of $p_{01}$ and $T_{01}$) of -0.51% and -0.41% were measured using the data acquired at the exit near and far planes respectively. The mass-averaged turbine efficiency values at the near plane were higher than those evaluated at the far plane (by ~0.4%) because the non-uniformities in total pressure were greater at the near plane due to less mixing. That is, $\bar{p}_{03}/\bar{p}_{01} > \bar{p}_{04}/\bar{p}_{01}$, and hence $\eta_{near,mass} > \eta_{far,.mass}$.

Agreement between the mixed-out values of efficiency at the near and far planes was expected. At the turbine exit far plane, partial mixing arose as a result of physical processes before the flow was fully mixed using the mixing model. With uniform inlet conditions, the near and far plane mixed-out turbine efficiency values agreed to within 0.13%. With inlet hot-streaks, the agreement was to within 0.07%.

With the introduction of inlet hot-streaks, the changes in the mixed-out (Dzung) turbine efficiencies using data acquired at the near and far planes were -0.88% and -0.68% respectively. The mean change mixed-out turbine efficiency was -0.78%.

The differences between the mass-averaged and mixed-out efficiencies also provided a measure of the secondary kinetic energy within the rotor exit flow-field. After mixing, the flow-field will only contain the kinetic energy that the mixing model considers useful. As the mixing model by Dzung mixes the area profile, the effects of the severe radial temperature distribution with inlet hot-streaks will be considered as useful kinetic energy. This would be appropriate from a design point of view. The differences between the mass-averaged and mixed-out turbine efficiency values at the near and far planes increased from 0.52% and 0.23% respectively with uniform inlet conditions to 0.89% and 0.50% respectively with inlet hot-streaks. This indicated that the rotor exit flow-field contained additional secondary kinetic energy with inlet hot-streaks.

With the introduction of inlet hot-streaks, an increase in shaft torque, and consequently shaft power, of 0.47% was measured. An increase in the isentropic turbine power by 0.81% resulted from increases in the stage mass flow rate, total-to-total pressure ratio and mass-averaged value of $c_p$ of 0.94%, 0.65% and 0.30% respectively. A decrease in the correction for non-adiabatic conditions by 0.34% resulted predominantly from a decrease in the vane heat transfer (see Qureshi *et al*. [21]). This was primarily caused by lower heat transfer to the vane row endwalls as a result of a greatly reduced driving temperature with the introduction of the hot-streak temperature profile at the vane inlet.

The variations in stage mass flow rate and shaft torque, and the attenuation of the temperature profile through the turbine stage and causes for the extra loss generation with inlet hot-streaks are discussed in the following sections. As the inlet temperature distortion was pronounced in the radial direction and relatively weak circumferential direction, the changes caused by introducing this inlet hot-streak profile were investigated using radial analyses that divided the flow passages into radial strips of equal span.

## IMPACT ON STAGE CAPACITY

At the MT1 design conditions, the stage mass flow rate is predominantly controlled by the near-choked vane row, and is proportional to the throat capacity, Γ, and inlet total pressure, and inversely proportional to the square-root of inlet total temperature. Neglecting changes in $\gamma$ and $R$, the capacity of the vane throat is a function of the effective area of the vane throat and static-to-total pressure ratio across the vane row, $p_2/p_{01}$.

The effective area of the vane throat is governed by vane aerodynamics. Munk and Prim [5] derived that no additional secondary flows are generated by inlet total temperature distortion in the static vane passage, provided that the distribution of inlet total pressure remains unaltered. To verify this experimentally, measurements of static pressure on the vane surfaces at 10%, 50% and 90% of the radial span were conducted with and without inlet temperature distortion. The results were processed to isentropic Mach number and are compared in Figure 7 below. These results confirmed that the aerodynamic performance of the vane row was unaffected by the introduction of inlet temperature distortion.

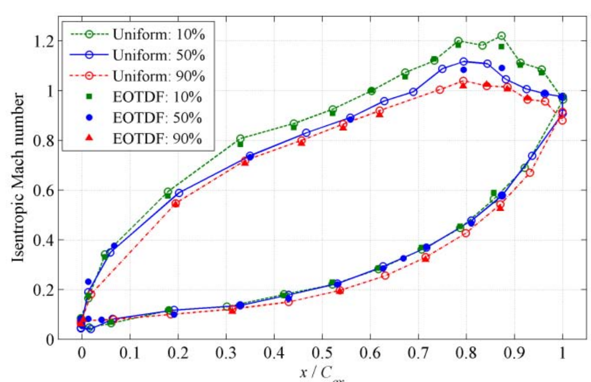


**FIGURE 7: Distributions of NGV surface isentropic Mach number with and without inlet temperature distortion**

To reconcile the measured change in stage mass flow rate with inlet temperature distortion, a radial strip analysis – the vane passage was divided into 20 radial strips of equal span – was performed to estimate the influence of altering the inlet total temperature profile and vane pressure ratio on the vane mass flow rate. This analysis is summarised by the plots in Figure 9. The spanwise variation in $p_2/p_{01} = f(r)$ was assumed linear between the measured values on the hub and casing endwalls. The static pressures on the hub and casing endwalls at the vane exit were each measured at five pitchwise locations. At the matched condition of $N/\sqrt{T_{01}}$, the measured changes in $p_2/p_{01}$ on the hub and casing endwalls were -0.49% and -0.76% respectively.

A typical experimental trend for the capacity of a modern HP turbine vane was presented by Povey et al. [25] and is also shown in Figure 8. Using this trend for vane capacity and $p_2/p_{01} = f(r)$, the change in vane capacity as a function of radial span, $\Delta\Gamma(r)$, was determined. The changes in the radial distribution of capacity due to the decrease in pressure ratio alone were small at less than 0.15%. The area-averaged change in capacity due to the change in pressure ratio alone was approximately 0.064%.

The radial profiles of inlet total temperature, $T_{01}(r)$, were taken as the circumferential averages of the area-survey data. These profiles were offset (by less than ±2K) to ensure that the mass-averaged inlet total temperature was consistent at 444 K. For the purpose of mass-averaging, the radial profile of mass flow rate was calculated using $p_2/p_{01} = f(r)$, $T_{01}(r)$ and the computed radial distribution of vane exit whirl angle from the Rolls-Royce through-flow code Q263. The change in the mass-averaged global value of $\sqrt{T_{01}}$ was -0.17%.

Mass flow rate is inversely proportional to the square-root of the local static temperature. Therefore, an effect of the inlet temperature distortion was to re-distribute mass into the endwall regions where $T_{01}$ was lower and the vane exit whirl

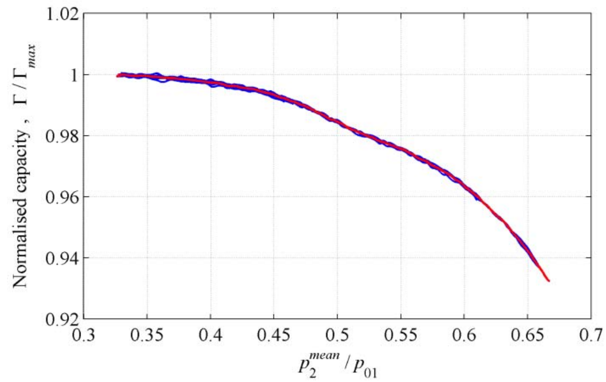


**FIGURE 8: Measured capacity of modern HP vane [25].**

distribution – whirl angle lower at endwalls – resulted in higher values of local capacity. Thus, the mass-averaged capacity was increased by +0.98%, while the average increase in local capacity was only +0.064%.

The predicted increase in mass-averaged capacity due to mass re-distribution resulted in a predicted increase in mass flow rate by 1.10%, which compared well with the measured change of +0.94%. It is work remarking that this effect is whirl distribution specific, and that for a flat (constant) whirl angle profile very little change in capacity or mass flow rate would be expected. However, the design of the MT1 HP vane can be regarded as fairly typical. It is also interesting to note that despite significant changes in incidence in the rotor frame of reference (see Figure 12), for a fixed stage pressure ratio, $p_3/p_{01}$, there was relatively little change in the vane pressure ratio, $p_2/p_{01}$, and this was not influential in this case.

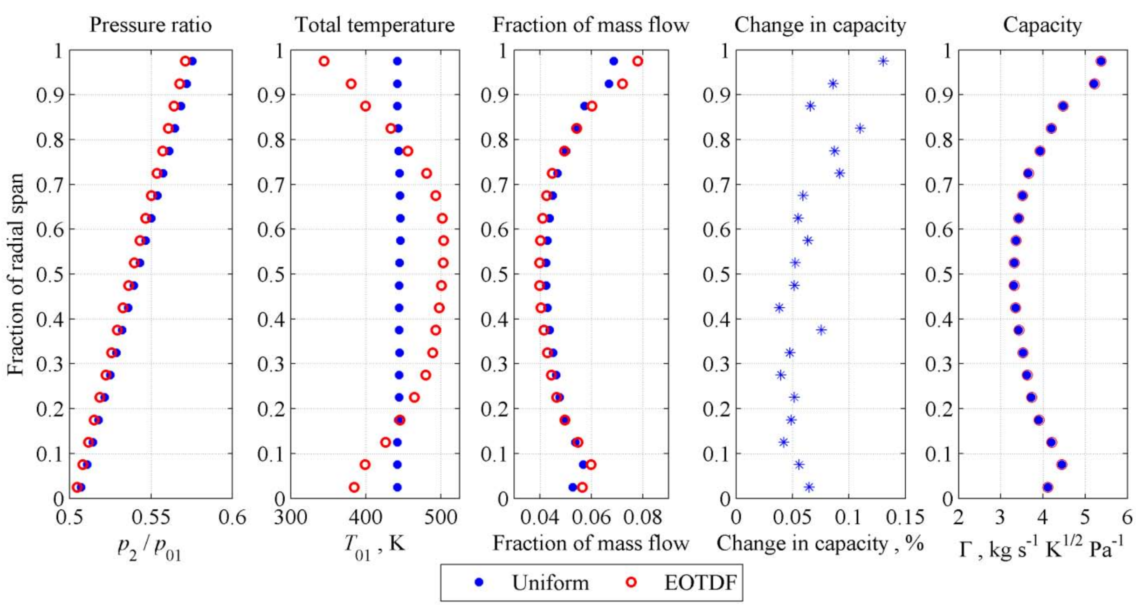


**FIGURE 9: Radial analysis of the effect of inlet temperature distortion on vane capacity**

## IMPACT ON SHAFT TORQUE

The radial distribution of the work extraction by the rotor can be expressed by the work function (also known as the blade loading coefficient):

$$\psi = \frac{(C_w)_2 - (C_w)_3}{U} = \frac{V_2 \sin(\alpha_2) - V_3 \sin(\alpha_3)}{U} \qquad (7)$$

where the absolute whirl angle, $\alpha$, is referenced to the axial direction and defined as positive in the direction of the vane turning (clockwise viewed from upstream). Absolute flow velocity is proportional to the square-root of the local static temperature and Mach number. With an unaltered aerodynamic behaviour within the vane passage with the introduction of inlet hot-streaks – see Figure 7 – it could be assumed that the vane exit absolute whirl angle, $\alpha_2$, and Mach number distributions were also unaltered.

The change in stage work function with the introduction of inlet hot-streaks was estimated using a radial strip analysis (20 strips). The radial distributions of absolute whirl velocity at the rotor inlet and exit were calculated from radial distributions of absolute Mach number, whirl angle and total temperature at these locations. At the rotor inlet, the radial distributions of Mach number and whirl angle computed by the Rolls-Royce through-flow code Q263 were used, and assumed unaffected by the introduction of inlet hot-streaks. The radial profiles of total temperature were assumed to be unaltered through the vane passage – justified later using Hydra CFD results. At the rotor exit the radial profiles were defined as the circumferential average of the experimental area-survey data. The calculated radial distributions of absolute whirl velocity at the rotor inlet and exit are plotted in Figure 10.The changes in these profiles with the introduction of inlet hot- streaks are also plotted. At the rotor inlet, the variation in the local static temperature with inlet hot-streaks resulted in changes in the absolute whirl velocity of approximately +20 $ms^{-1}$ and -35 $ms^{-1}$ at the mid-span and endwalls respectively. Lower changes were calculated at the rotor exit, typically less than ±10 ms-1. Therefore, the changes in the radial distribution of work function – also plotted in Figure 10 – were predominantly driven by the changes in absolute whirl velocity at the rotor inlet, which was caused by altering the vane exit static temperature field with the introduction of inlet hot-streaks. The largest local change in work function was approximately -20% at the casing wall. The changes at mid-span and the hub wall were approximately +5% and -5% respectively.

The radial profiles of mass flow rate at the vane exit, computed by the radial strip analysis detailed in the previous section (plotted as a fraction of the stage mass flow rate in Figure 9) were used to calculate the values of mass-averaged work function and shaft torque with and without inlet hot-streaks. The calculated radial profiles for the extraction of shaft torque are plotted in Figure 10. The mass-averaged change in work function with the introduction in inlet hot-streaks was calculated at -0.52%. The estimated global change in shaft torque with the introduction of inlet hot-streaks was +0.26%, which compared well with the measured change of +0.47%.

In summary, the introduction of inlet hot-streaks greatly altered the radial work function distribution for the turbine stage. This variation predominantly resulted from changes in the static temperature field at the vane exit which caused the distribution of absolute whirl velocity at the rotor inlet to be altered. Although the work function at mid-span was increased with inlet hot-streaks by increasing the local static temperature, the re-distribution of mass towards the endwalls and into a region of decreased work function caused the mass-averaged work function value to decrease by -0.52%. However, the increase in stage mass flow rate with inlet hot-streaks caused a global increase in shaft torque by +0.47%.

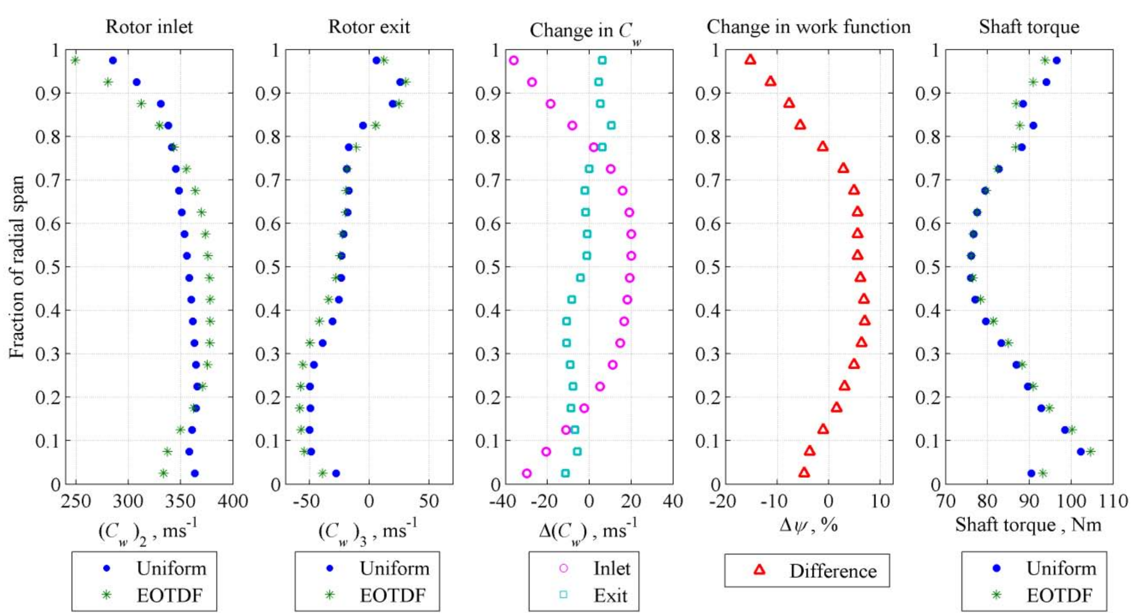


**FIGURE 10: Calculated differences in radial work function distribution with inlet hot-streaks**

## ATTENUATION OF TEMPERATURE PROFILE

As a hot-streak temperature profile travels through a turbine stage, the profile is attenuated by non-uniform work extraction – see Figure 10 – and re-distribution and mixing.

The measured radial profiles (circumferential averages of the area-survey data) of total temperature and rotor exit near and far planes are shown in Figure 11 below. Using this data and the radial distributions $T_{01}$ and work function plotted in Figure 9 and Figure 10 respectively, the hot-streak attenuation was separated and quantified between that resulting from flow re-distribution/mixing and work extraction. Assuming that no flow re-distribution/mixing occurred in the stage, the drop in total temperature across the stage can be calculated as:

$$\Delta T_{0,\psi} = \psi U^2 / c_p = \{(C_w)_2 + (C_w)_3\}\, U / c_p \tag{8}$$

Using this definition, the radial profile of total temperature at the rotor exit that would result with solely work extraction was calculated as $T_{01}(r) - \Delta T_{0,\psi}(r)$. Likewise, the radial profile of total temperature at the rotor exit far plane that would result from solely flow re-distribution/mixing was calculated as $T_{04}(r) + \Delta T_{0,\psi}(r)$. With these profiles defined, a profile attenuation factor, $\alpha_{profile}$, was defined as:

$$\alpha_{profile} = 1 - \frac{(T_{max} - T_{min})_{exit}}{(T_{max} - T_{min})_{inlet}} \tag{9}$$

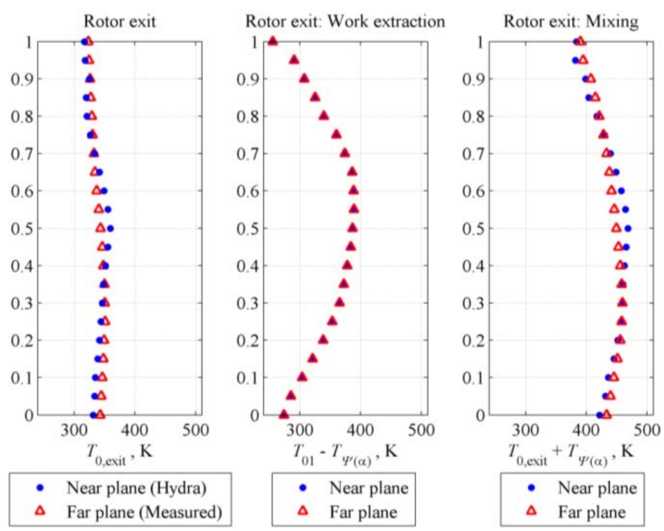


**FIGURE 11: Attenuation of radial temperature profile by work extraction and flow re-distribution/mixing**

A summary of the calculated profile attenuations are presented in Table 3 below. Using the definition above, the change in $\alpha_{profile}$ between stage inlet and rotor exit far plane was 0.841. Of this, non-uniform work extraction accounted for a change of 0.231 and mixing accounted for 0.610. The change due to mixing between the rotor exit near and far plane was 0.086.

| Temperature profile | $T_{max}$ | $T_{min}$ | $T_{max} - T_{min}$ | $\alpha_{profile}$ |
|---|---|---|---|---|
| Inlet plane, $T_{01}$ | 496.4 K | 322.5 K | 173.9 K | 0 |
| Exit far plane, $T_{04}$ | 350.8 K | 323.2 K | 27.6 K | 0.841 |
| Work extraction, $T_{01} - \Delta T_{0,\psi}$ | 388.8 K | 255.0 K | 133.8 K | 0.231 |
| Flow re-distribution/ mixing, $T_{04} + \Delta T_{0,\psi}$ | 459.1 K | 391.2 K | 67.9 K | 0.610 |
| Exit near plane, $T_{03}$ | 359.5 K | 316.9 K | 42.6 K | 0.755 |

**TABLE 3: Attenuation of EOTDF temperature profile**

At the rotor exit far plane, a significant radial temperature profile with a $T_{max}/T_{min}$ of 1.08 remained. If a row of downstream vanes were designed for the (mass) averaged HP rotor exit temperature, the performance of the downstream stage might not be optimised and local over-heating of the vane surfaces may occur.

## LOSS GENERATION WITH EOTDF

The difference between the mass-averaged and mixed-out turbine efficiency is greater with inlet hot-streaks than without. This suggests an increase in secondary loss, and is consistent with the measured decrease in turbine efficiency.

It is accepted that the introduction of gradients of inlet total temperature will not – in the absence of changes in the total pressure field – cause additional loss generation in the vane row. In the current experiment emphasis was placed on achieving a flat total pressure profile for both EOTDF and uniform inlet runs. In the rotor, however, the introduction of EOTDF causes an increase in relative-frame radial total pressure variation and whirl variation at rotor inlet. This results in off-design incidence and is likely to lead to enhanced secondary flow.

The impact of off-design incidence on the rotor performance with inlet hot-streaks was estimated using the correlation for profile loss at off-design conditions by Benner *et al*. [26]. The spanwise changes in profile loss were calculated by applying this correlation at a number of spanwise locations. The radial profiles of relative whirl angle at the rotor inlet, $\beta_{2,rel}$, with uniform inlet conditions and inlet hot-streaks were calculated using the circumferential averages of the measured inlet total temperature profiles, and the radial profiles of vane exit Mach number and absolute whirl angle from the Rolls-Royce through-flow code Q263. The calculated changes in relative whirl angle at the rotor inlet with EOTDF are plotted in Figure 12. The predicted change in profile loss coefficient, $Y_p$, and the impact on efficiency (using mean-line loss correlation by Kacker and Okapuu [27]) are also plotted.

Changes in $\beta_{2,rel}$ of approximately +5°, -10° and - 20° were calculated at mid-span, hub and casing respectively. The estimated mass-averaged change in turbine efficiency due to additional profile loss with EOTDF in the rotor using this method was -0.07%. This corresponded to approximately 10% of the mean measured change in mixed-out turbine efficiency.

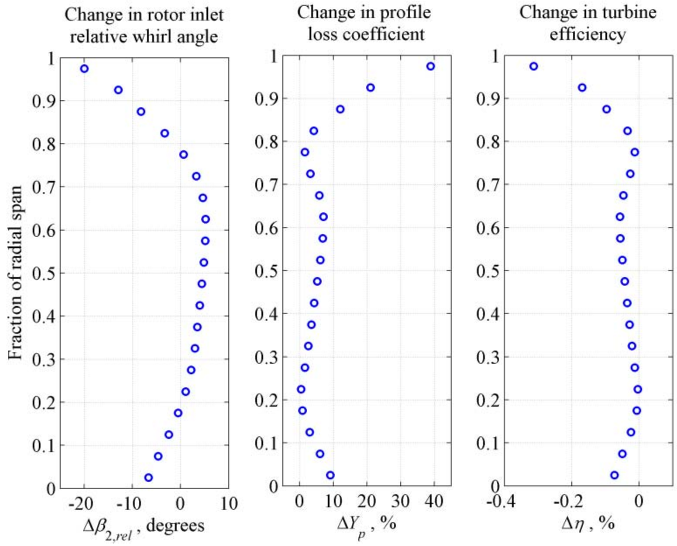


**FIGURE 12: Predicted impact of off-design incidence on rotor performance with EOTDF – differences plotted as changes from case with uniform inlet conditions**

Hawthorne [7] showed that additional secondary flows are generated in a rotating blade row with the presence of strong density gradients, as well as from gradients in rotary pressure defined as $p_{0,R} = p_{0,rel} - 0.5\rho U^2$. With EOTDF, increased radial gradients in total temperature at the rotor inlet plane significantly alter the radial gradients in density and rotary total pressure at this station. As expected, this appears to lead to additional generation of secondary vorticity.

By assuming an axi-symmetric flow-field and small gradients in the axial direction, Butler *et al*. [4] simplified the expression for the production of streamwise vorticity in a steady, incompressible flow derived by Hawthorne [7] to:

$$r\frac{\partial}{\partial s}\left(\frac{\Omega_S}{w}\right) = \frac{2}{\rho w^2}\left(\frac{\partial p_{0,R}}{\delta r} + \frac{U^2}{2}\frac{\partial \rho}{\partial r}\right) \sim \frac{2}{\rho w^2}\left(\frac{\partial p_{0,rel}}{\partial r}\right) \qquad (10)$$

The spanwise profiles of density and rotary total pressure at the rotor inlet with uniform inlet conditions and inlet hot-streaks are plotted in Figure 13. These data were calculated assuming that the circumferentially averaged inlet total temperature profiles were unaltered through the vane passage, and that the spanwise profiles of Mach number and absolute whirl angle were unaffected by the introduction of inlet hot-streaks. For both test cases, the spanwise distribution for the rate of production of streamwise vorticity, given by the right-hand-side (RHS) of equation (10), is also plotted in Figure 13. For this purpose, a simple central difference scheme was used to determine gradients. The mean of the absolute values for the profiles of equation (10) were 0.009 and 0.013 with uniform inlet conditions and inlet hot-streaks respectively. A predicted increase in vorticity production with EOTDF is consistent with the measured increase in secondary kinetic energy at the rotor exit. In the experiment, this was indicated by a greater difference between the mass-averaged and mixed-out values of turbine efficiency with EOTDF.

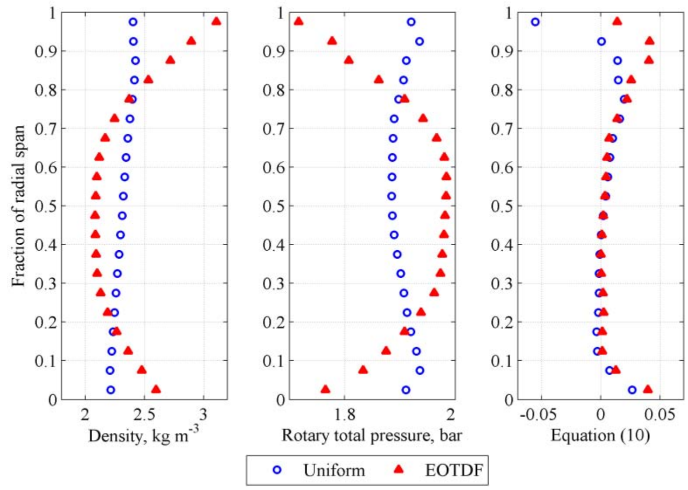


**FIGURE 13: Generation of streamwise vorticity by gradients in rotor inlet flow-field**

## COMPUTATIONAL RESULTS

CFD predictions were performed to aid interpretation of experimental results and to verify assumptions used in the analysis of the experimental data.

The measured and computed (time-averaged) distributions of vane surface isentropic Mach number at 50% of the radial span with inlet hot-streaks are compared in Figure 14. The computed distribution with uniform inlet conditions is also plotted to evaluate any changes predicted by the computation. There is excellent agreement between prediction and experiment for the case of EOTDF, and no predicted change in vane aerodynamics between uniform and EOTDF cases. This agrees with the experimental findings and the substitution principle by Munk and Prim [5]. Similar agreement was also found between the data at 10% and 90% of the radial span. The redistribution of rotor capacity clearly has little impact on the vane aerodynamics.

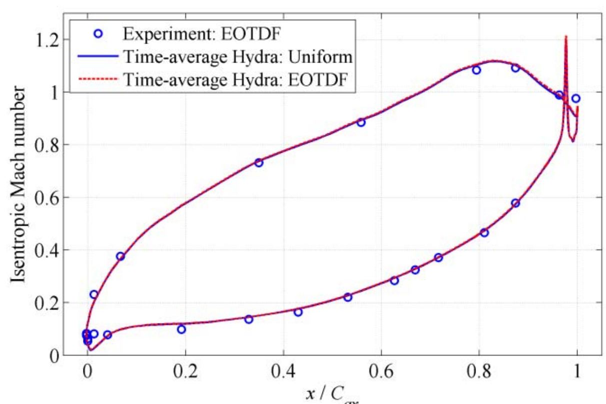


**FIGURE 14: Computed NGV isentropic Mach number distributions at 50% span with and without inlet hot-streaks**

In the analysis of the experimental data a number of assumptions were made concerning the nature of the flow-field at the vane exit. Firstly, it was assumed that the radial profile of vane inlet total temperature was unaltered through the vane passage. The computed radial profiles (circumferential averages) of total temperature at the vane inlet and exit with inlet hot-streaks are plotted in Figure 15. The data showed only a slight radial migration of hot gas towards the hub endwall in the vane passage. This was caused by inward streamline curvature close to the vane suction surface near its trailing edge, (present for both inlet boundary conditions).

It was also assumed that the profiles of vane exit absolute whirl angle and Mach number were unaltered with EOTDF. The computed changes are plotted in Figure 15. The predictions confirmed that neither of these profiles was manifestly affected by the introduction of inlet hot-streaks. The maximum changes in vane exit whirl angle and Mach number were -0.5° and -0.003 respectively.

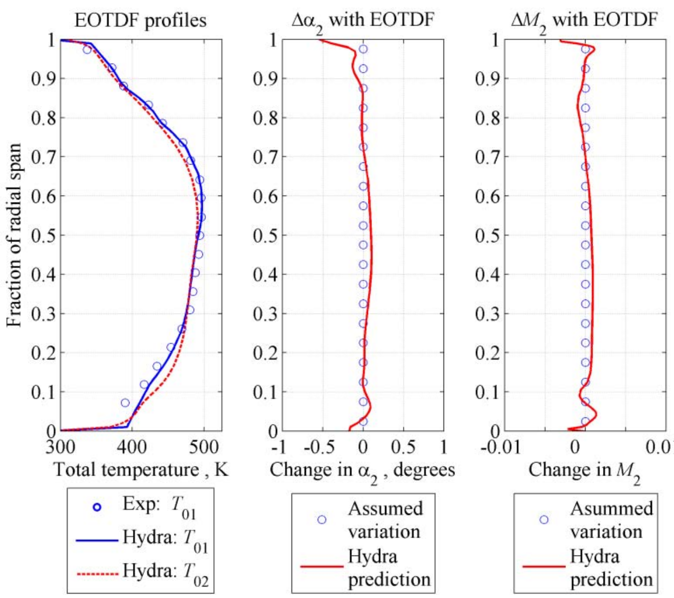


**FIGURE 15: Computed profiles of vane inlet and exit total temperature, and computed changes in vane exit whirl angle and Mach number with inlet hot-streaks**

For each of the inlet boundary conditions, the computed radial profiles (circumferential averages) of relative total temperature and pressure at the rotor inlet are compared to those calculated with the stated assumptions in Figure 16 and Figure 17 respectively. The percentage differences (from the case with uniform inlet conditions) in these profiles between to the two test cases are also plotted. The computed and calculated profiles of both relative total temperature and pressure compared well. The small under-calculation of relative total temperature below 30% of the radial span with inlet hot-streaks resulted from the computed radial inward migration of hot gas in the vane passage.

Good agreement between these data is seen as justification of the assumptions used in the experimental data analysis. That is, the main aerodynamic changes arising from EOTDF introduction can largely be predicted using a simple radial strip analysis based on velocity triangles (little 3d flow).

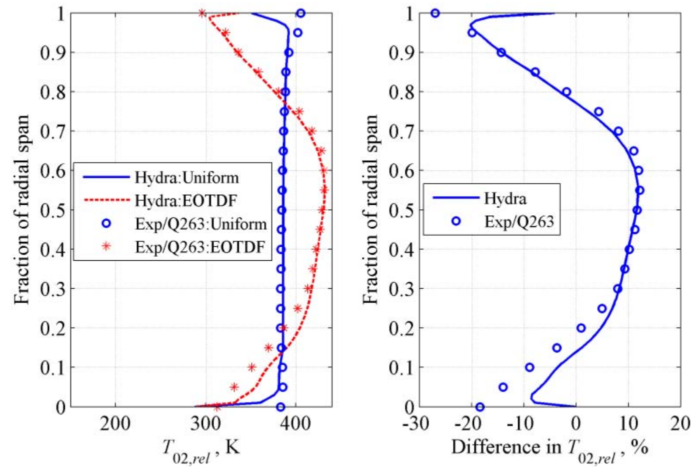


**FIGURE 16: Computed changes in relative total temperature at rotor inlet with inlet hot-streaks**

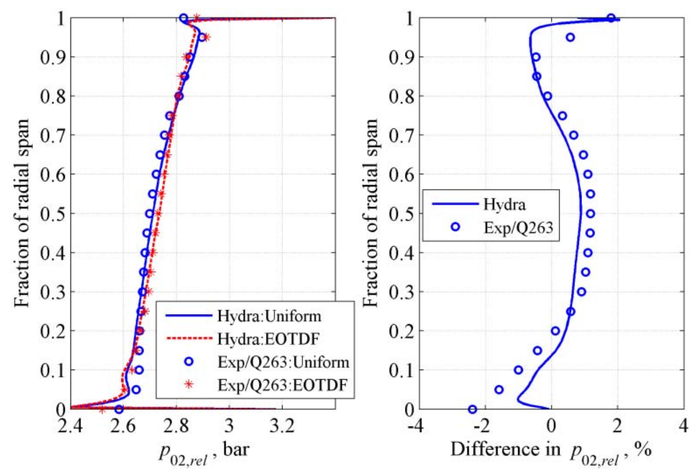


**FIGURE 17: Computed changes in relative total pressure at rotor inlet with inlet hot-streaks**

The impact of introducing inlet hot-streaks on the mass-averaged value of turbine efficiency was also calculated from the computational results. The results for both the steady and unsteady computations are compared to the experimental results in Table 4. The computed changes in stage pressure total-to-total pressure ratio, mass flow rate, specific work and turbine efficiency all matched in trend with the experimental results. The predicted changes in stage pressure ratio were +0.41% (steady) and +0.24% (unsteady). These agree reasonably well with the measured change of +0.51%. The measured change in specific work was -0.48%. The predicted changes were -0.19% (steady) and -0.22% (unsteady). The computed changes in stage capacity were both approximately +0.11%. This was an under-prediction by approximately 0.8% from the measured change. It is believed that this discrepancy was predominantly caused by small errors in the predicted vane exit whirl angle profile.

The computed changes in mass-averaged turbine efficiency were -0.14% (steady) and -0.27% (unsteady). The change predicted by the unsteady computation agreed reasonably well with the measured change of -0.51%.

| Parameter | Experiment | Steady | Unsteady |
|---|---|---|---|
| $\bar{p}_{03}/\bar{p}_{01}$ | +0.51% | +0.42% | +0.24% |
| Mass flow rate, $\dot{m}$ | +0.94% | +0.10% | +0.11% |
| Specific work | -0.48% | -0.19% | -0.22% |
| $\eta_{mass,near}$ | -0.51% | -0.14% | -0.27% |

**TABLE 4: Summary of computed turbine efficiency**

## CONCLUSIONS

The impact of introducing engine-representative inlet temperature distortion (hot-streaks) on the efficiency of a modern unshrouded high-pressure turbine stage has been investigated. This study was conducted in Oxford Turbine Research Facility (OTRF) with an efficiency measurement system capable of resolving changes in turbine efficiency to within ±0.16%.

Engine manufacturers commonly design turbine stages using CFD with uniform inlet boundary conditions of pressure and temperature. The research was performed under matched engine conditions with engine-representative inlet hot-streaks, so the measured changes in turbine efficiency can be taken as a guide to the difference between that achieved in practice and predicted in simple calculations.

Turbine efficiency was evaluated based on data acquired at two turbine exit planes (*near* and *far* planes). The changes in mixed out efficiency with temperature distortion using these data were -0.88% (near) and -0.68% (far).

The experiments demonstrated that the aerodynamic behaviour of the HP vane was unaffected by temperature distortion. For the rotor, however, the hot-streak profile resulted in off-design conditions of relative whirl angle, relative total pressure and density. Increased loss with temperature distortion was attributed to these off-design conditions.

The measured change in stage mass flow rate of +0.94% reconciled to within 0.16% of the value estimated from a spanwise vane capacity analysis. The change was caused by re-distribution of mass towards the hub and casing endwalls where the local value of capacity was higher. The measured change in shaft torque was +0.47%. A spanwise analysis estimated changes in shaft torque and mass-averaged work function to be +0.26% and-0.56% respectively. The decrease in work function was caused by the re-distribution of mass towards the endwalls, into regions of lower local work function.

Full-stage unsteady CFD was performed using the Rolls-Royce Hydra code. The results of the CFD were used to validate the simple radial strip approach to the analysis presented. It was demonstrated that this simple approach was capable of providing a reasonable approximation of inter-stage conditions with the introduction of inlet temperature distortion.

The computed change in turbine efficiency agreed with the experimental value to within 0.24%.

## NOMENCLATURE

| | |
|---|---|
| $B$ | Bias uncertainty |
| $c_p$ | Specific heat capacity, J kg$^{-1}$ K$^{-1}$ |
| $C_w$ | Absolute whirl velocity, m s$^{-1}$ |
| $h$ | Specific enthalpy, J kg$^{-1}$ |
| $\dot{H}$ | Enthalpy flux, W |
| $I_{rotor}$ | Moment of inertia of rotor disc, kg m$^2$ |
| $M$ | Mach number |
| $\dot{m}$ | Mass flow rate, kg s$^{-1}$ |
| $N$ | Rotational speed, rpm |
| $p$ | Pressure, Pa |
| $q$ | Specific heat transfer, J kg$^{-1}$ |
| $\dot{Q}$ | Heat transfer rate, W |
| $r$ | Radius, m |
| $Re$ | Reynolds number |
| $s$ | Specific entropy, J kg$^{-1}$ K$^{-1}$ |
| $S$ | Precision uncertainty |
| $T$ | Temperature, K |
| $T_{gauge}$ | Torque experienced at strain gauge location, Nm |
| $T_{rotor}$ | Torque exerted by rotor blades, Nm |
| $T_{wind}$ | Windage torque, Nm |
| $U$ | Blade speed ,m s$^{-1}$ |
| $V$ | Absolute flow velocity, m s$^{-1}$ |
| $w$ | Specific work, J kg$^{-1}$ |
| $\dot{W}$ | Power, W |
| | |
| $\alpha$ | Absolute whirl angle, degrees |
| $\gamma$ | Ratio of specific heats |
| $\Gamma$ | Capacity, kg s$^{-1}$ K$^{1/2}$ Pa$^{-1}$ |
| $\eta$ | Efficiency |
| $\psi$ | Work function (or blade loading coefficient) |
| $\omega$ | Rotational velocity, rad s$^{-1}$ |
| $\dot{\omega}$ | Rotational acceleration, rad s$^{-2}$ |
| | |
| 0 | Stagnation, or total, conditions |
| 1 | Conditions at inlet to nozzle guide vane |
| 2 | Conditions at exit of nozzle guide vane/rotor inlet |
| 3 | Conditions at rotor exit near plane |
| 4 | Conditions at rotor exit far plane |
| $actual$ | Actual value |
| $BL$ | Value resulting from boundary layer growth |
| $cold$ | Cold gas value |
| $EOTDF$ | Enhanced Overall Temperature Distortion Factor |
| $far$ | Value referenced to rotor exit far plane |
| $gas$ | Free-stream gas value |
| $hot$ | Hot gas value |
| HP | High-pressure |
| HT | Non-adiabatic value |
| $ideal$ | Value resulting from ideal reference process |
| IP | Intermediate-pressure |

| | |
|---|---|
| *is* | Value resulting from isentropic reference process |
| LP | Low-pressure |
| *near* | Value referenced to rotor exit near plane |
| NGV | Nozzle guide vane |
| *wall* | Wall value |


## ACKNOWLEDGEMENTS

The authors would like to acknowledge the financial support of the European Union and European manufacturers that participated in the Project TATEF II "Turbine Aero-Thermal External Flows II." Particular thanks go to the staff at QinetiQ for their contributions during the test programme.


## REFERENCES


[1] Dorney, D.J., Gundy-Burlet, K.L., and Sondak, D.L., 1999, "A survey of hot-streak experiments and simulations," International Journal of Turbo and Jet Engines, Vol. 16, pp. 1-15.

[2] Povey, T., Chana, K.S., Jones, T.V., and Hurrion, J., 2007, "The effect of hot-streaks on HP vane surface and endwall heat transfer: an experimental and numerical study," Transactions of the ASME Journal of Turbomachinery, Vol. 129, January 2007, pp 32-43.

[3] Povey, T., and Qureshi, M.I., 2009, "Developments on hot-streak simulators for turbine testing," Transactions of the ASME Journal of Turbomachinery Vol.131, Issue 3, July 2009, 031009.

[4] Butler, T.L., Sharma, O.P., Joslyn, H.D., and Dring, R.P., 1989, "Redistribution of an inlet temperature distortion in an axial flow turbine stage," AIAA Journal of Propulsion and Power, Vol. 5, No. 1, pp 64-71.

[5] Munk, M., and Prim, R.C., 1947, "On the multiplicity of steady gas flows having the same streamwise pattern," Proceeding s of the National Academy of Science, U.S.A., Vol. 33, pp 137-141.

[6] Kerrebrock, J.L., and Mikolajczak, A.A., 1970, "Intra-stator transport of rotor wakes and its effects on compressor performance," Journal of Engineering Physics, Vol. 92, No. 4, pp. 359-368.

[7] Hawthorne W.R., 1974, "Secondary Vorticity in Stratified Compressible Fluids in Rotating Systems," CUED/ATurbo/TR63. University of Cambridge Department of Engineering.

[8] Shang, T., Guenette, G.R., Epstein, A.H., and Saxer, A.P., 1995, "The influence of inlet temperature distortion on rotor heat transfer in a transonic turbine," 31st AIAA/ASME/SAE/ASEE Joint Propulsion Conference and Exhibit, AIAA Paper 95-3042, July 10-12, San Diego, CA.

[9] Shang, T., and Epstein, A.H., 1997, "Analysis of hot streak effects on turbine rotor heat load," Transactions of the ASME Journal of Turbomachinery, Vol. 119, July.

[10] Chana, K.S., and Jones T.V., 2002, "An investigation on turbine tip and shroud heat transfer," ASME Paper Number GT-2002-30554.

[11] Povey, T., Chana, K.S., and Jones, T.V., 2003, "Heat transfer measurement on an intermediate pressure nozzle vane tested in a rotating annular turbine facility – and the modifying effects of a non-uniform inlet temperature profile," Proceedings of the Institute of Mechanical Engineers, Vol. 217, Part A: Journal of Power and Energy, pp 421-431.

[12] Qureshi, M.I., Povey, T., Smith, A., and Chana, K.S., 2010, "Effect of temperature nonuniformity on heat transfer in an unshrouded transonic HP turbine: an experimental and computational investigation," Journal of Turbomachinery; No. TURBO-10-1091.

[13] Jones, T.V., Schultz, D.L., and Hendley, A., 1973, "On the flow in an isentropic light piston facility," Ministry of Defence, Aeronautical Research Council, R & M Number 3731.

[14] Goodisman, M.I., Oldfield, M.L.G., Kingcombe, R.C., Jones, T.V., Ainsworth, R.W., and Brooks, A.J., 1992, "An Axial Turbobrake," Transactions of the ASME Journal of Turbomachinery, April 1992, Vol. 114, pp. 419-425.

[15] Povey, T., and Qureshi, M.I., 2008, "A hot-streak (combustor) simulator suited to aerodynamic performance measurements," Transactions of the Institution of Mechanical Engineers, Part G, Journal of Aerospace Engineering, Vol. 222, Number 6, pp. 205-220.

[16] Beard, P.F., Povey, T., and Chana, K.S., 2009, "Turbine efficiency measurement systems for the QinetiQ Turbine Test Facility," Transactions of the ASME Journal of Turbomachinery, Vol. 132, No.1, 011002.

[17] Beard, P.F., Povey, T., and Smith, A., 2011, "Efficiency of an unshrouded transonic HP turbine: Experimental measurements in a short duration facility and CFD predictions," Submitted to IMechE, Part A: Journal of Power and Energy.

[18] Beard, P.F., and Povey, T., 2011, "Direct shaft torque measurement in a transient turbine facility," Journal of Measurement Science and Technology, Vol. 22, No. 3, 035107, 10pp, doi: 10.1088/0957-0233/22/3/035107.

[19] Beard, P.F., Povey, T., and Ireland, P.T., 2008, "Mass flow rate measurement in a transonic test facility with temperature distortion and swirl," Journal of Flow Measurement and Instrumentation, Vol. 19, Issue 5, Oct, pp. 315-324, doi:10.1016/j.flowmeasinst.2008.03.004.

[20] Chana, K.S., and Hilditch, M.A., 1995, "A summary datum un-cooled measurements of the MT1 single stage high-pressure turbine in the DRA Pyestock Isentropic Light Piston Facility," IMT Area 3 Turbine Project AER2-CT92-0044 report (Also DRA/AS/PTD/TR95046/1).

[21] Qureshi, I., Beretta, A., Povey, T., 2010, "Effect of simulated combustor temperature non-uniformity on HP vane and endwall heat transfer: An experimental and computational investigation," Journal of Engineering for Gas Turbines and Power; No. GTP-10-1126.

[22] Atkins, N.A., and Ainsworth, R.W., 2007, "Turbine aerodynamic performance measurement under non-

adiabatic conditions," ASME Paper Number GT2007-27143.
[23] Lapworth, B. L., 2004, "HYDRA-CFD: A framework for collaborative CFD development," International Conference on Scientific and Engineering Computation IC-SEC 2004, 30th June – 2nd July, Singapore.
[24] Pianko, M., and Wazelt, F., 1983, "Suitable averaging-techniques in non-uniform internal flows," AGARD Advisory Report AGARD-AR-182.
[25] Povey, T., Sharpe, M., and Rawlinson, A., 2011, "Experimental measurements of gas turbine flow capacity using a novel transient technique," Transactions of the ASME Journal of Turbomachinery, Vol. 133, Issue 1, 011005, doi:10.1115/1.4000481.
[26] Benner, M.W., Sjolander, S.A., and Moustapha, S.H., 1997, "Influence of leading-edge geometry on profile losses in turbines at off-design incidence: Experimental results and an improved correlation," Transactions of ASME Journal of Turbomachinery, Vol. 119, pp. 193-200.
[27] Kacker, S.C., and Okapuu, U., 1982, "A mean line prediction method for axial flow turbine efficiency," Transactions of ASME Journal of Engineering for Power, Vol. 104, pp. 111-119.